Metastability of Au–Ge Liquid Nanocatalysts: Ge Vapor–Liquid–Solid Nanowire Growth Far below the Bulk Eutectic Temperature

Hemant Adhikari,[†,*] Ann F. Marshall,[‡] Irene A. Goldthorpe,[†] Christopher E. D. Chidsey,[§] and Paul C. McIntyre[†,‡]

[†]Department of Materials Science and Engineering, [‡]Geballe Laboratory for Advanced Materials, and [§]Department of Chemistry, Stanford University, Stanford, California 94305

ABSTRACT The vapor–liquid–solid mechanism of nanowire (NW) growth requires the presence of a liquid at one end of the wire; however, Au-catalyzed Ge nanowire growth by chemical vapor deposition can occur at ~100 °C below the bulk Au–Ge eutectic. In this paper, we investigate deep sub-eutectic stability of liquid Au–Ge catalysts on Ge NWs quantitatively, both theoretically and experimentally. We construct a binary Au–Ge phase diagram that is valid at the nanoscale and show that equilibrium arguments, based on capillarity, are inconsistent with stabilization of Au–Ge liquid at deep sub-eutectic temperatures, similar to those used in Ge NW growth. Hot-stage electron microscopy and X-ray diffraction are used to test the predictions of nanoscale phase equilibria. In addition to Ge supersaturation of the Au–Ge liquid droplet, which has recently been invoked as an explanation for deep sub-eutectic Ge NW growth, we find evidence of a substantial kinetic barrier to Au solidification during cooling below the nanoscale Au–Ge eutectic temperature.

KEYWORDS: sub-eutectic growth · phase diagram · nanowires · germanium · nanocatalyst · TEM · Au–Ge

One-dimensional structures such as nanotubes and nanowires are being investigated for various applications in nanotechnology, including nanoelectronics. In particular, silicon- or germanium-based nanowire devices are desirable for electronic and other applications because of their compatibility with Si integrated circuits. The potential of Ge nanowires (NWs) as building blocks for three-dimensional (3D) integrated circuits has been demonstrated by successful fabrication of field-effect transistors using p-type Ge NWs and a deposited high dielectric constant (high-*k*) film as gate insulator.[1] The relatively low growth temperature (<400 °C) needed for metal-catalyzed chemical vapor deposition (CVD) of Ge NWs[2–4] makes them compatible with 3D integrated circuit fabrication.

The widely accepted theory of nanowire growth *via* the vapor–liquid–solid (VLS) mechanism was first suggested by Wagner[5] for micrometer-sized silicon whiskers grown in the presence of gold impurities at 950 °C, which is well above the eutectic temperature of the Au–Si binary system. This mechanism has subsequently been used to explain the growth of nanowires with diameters as small as 10 nm.[3,6,7] In the VLS mechanism (Figure 1) the reactants are introduced *via* the vapor phase and decompose and/or dissolve into the catalyst to form a molten alloy of the catalyst and reactant species. Supersaturation of the molten droplet by Ge leads to nucleation and axial growth of a nanowire.

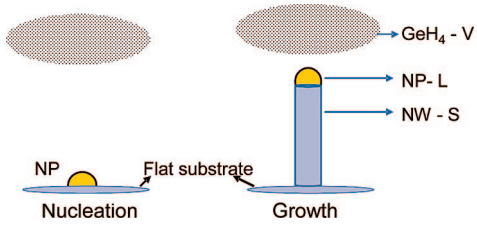

Figure 1. Schematic illustration of the vapor–liquid–solid (VLS) mechanism showing both nanowire nucleation and growth geometries.

The requirement of a liquid for the VLS mechanism suggests that nanowire growth should be carried out at temperatures above the binary eutectic melting point. In our previous work,[2] we found that nanowires grown at temperatures near the bulk eutectic are tapered because of uncatalyzed germanium deposition on the sidewalls of the growing nanowires at these high temperatures. Tapering of the nanowires is not desirable for many applications because nanowire device characteristics may be strongly dependent on nanowire diameter. We found that

*Address correspondence to h.adhikari@gmail.com.

Received for review August 6, 2007 and accepted November 20, 2007.

Published online December 28, 2007.
10.1021/nn7001486 CCC: $37.00

temperatures close to the bulk eutectic of the Au−Ge binary system (360 °C) were required for efficient nucleation of epitaxial nanowires on Ge single-crystal substrates. However, after cooling from this nucleation step, the subsequent growth of single-crystal nanowires could be carried out at temperatures as low as 90 °C below the eutectic.[2] Transmission electron microscopy (TEM) studies of these nanowires indicate that there is no substantial difference in their crystalline quality or orientation for wires grown at temperatures near the bulk eutectic compared to those grown at very large undercoolings. Moreover, we observe relatively high Ge NW growth velocities which are weakly dependent on temperature below the bulk eutectic, which is further evidence of a single growth mechanism in our experiments. Therefore, we find no evidence for a transition to a different growth mechanism [*e.g.*, a transition from VLS to vapor–solid–solid (VSS) growth] on cooling after Ge NW nucleation. Recent *in situ* TEM studies of Ge nanowire CVD have, in fact, shown that VSS growth of Ge nanowires can occur, but at velocities 1−2 orders of magnitude slower than VLS at the same temperature.[8]

There are several other reports of nanowire growth well below the relevant eutectic temperatures.[3,6,8–10] It has sometimes been suggested[3] that capillary effects, which result in melting point depression for elemental nanoparticles,[11] can account for the depression of the binary eutectic temperature in these systems. Capillary effects, often represented by the Gibbs–Thomson pressure, increase the free energy of single-component nanoparticles relative to the bulk values and thus cause a reduction in their melting temperatures. A better understanding of binary Au−Ge phase equilibria at nanometer-scale dimensions is required to determine the extent to which capillary effects (1) alter the stability of the binary liquid, (2) contribute to the driving force for Ge transfer from a Au−Ge liquid to the Ge NW tip, and (3) influence the driving force for final nucleation of the Au(s) catalyst at the termination of growth. These calculations are thus invaluable for understanding deep sub-eutectic solidification quantitatively.

In principle, the Gibbs–Thomson effect may either increase or decrease the equilibrium melting point in a binary eutectic system, depending upon the surface energies and molar volumes of the two solid components and the liquid phase. A better understanding of Au−Ge phase equilibria at nanometer-scale dimensions is required to determine the extent to which capillary effects contribute to the stability of a liquid catalyst particle during low-temperature nanowire growth. We have calculated equilibrium phase diagrams for the Au−Ge binary in the nanometer-scale regime. The bulk equilibrium phase diagram for Au−Ge was reported by Okamoto and Massalski in 1984[12] and can be calculated using the Gibbs free energy of the face-centered-cubic (fcc; Au-rich) solid solution, the liquid solution, and the diamond-cubic structure Ge published therein. Effective Gibbs–Thomson pressures acting on the catalyst particle (both in solid and liquid form) and the Ge NW are proportional to the product of their surface curvature and surface energy.[13] These pressure terms increase the free energy of the nanoscale catalyst and the nanowire relative to the bulk values. To calculate the capillary increase in the Gibbs free energy of the various phases, one needs to estimate the surface energy of the non-ideal multicomponent liquid and solid solutions of Au and Ge.

We have assumed a monolayer model in which the discontinuity in surface properties of a condensed phase is confined to a single monolayer at its surface. The surface energy, σ, is modeled with the following equation:

$$\sigma A = G^{(m)} - \sum_{i=1}^{p} n_i^{(m)} \mu_i \qquad (1)$$

where A is the surface area, $G^{(m)}$ is the Gibbs free energy of the surface monolayer, $n_i^{(m)}$ is the number of moles of component i in the monolayer, and μ_i is the chemical potential of this component in the adjacent phases, which depends on the temperature, pressure (including capillary pressure), and composition. Equation 1 is reasonable from an intuitive perspective, and it can also be derived through a variational analysis of the kind described by Butler.[14] The approach for determining the surface energy of multicomponent alloys is described in detail in the Supporting Information (section S1). The surface energy σ of the Au−Ge binary alloy can be expressed as

$$\sigma = \sigma_{Ge}^{0} + \frac{RT}{\alpha_{Ge}} \ln\left(\frac{X_{Ge}^{(m)}}{X_{Ge}}\right) + \frac{G_{Ge}^{xs,(m)} - G_{Ge}^{xs,B}}{\alpha_{Ge}} = \sigma_{Au}^{0} + \frac{RT}{\alpha_{Au}} \ln\left(\frac{X_{Au}^{(m)}}{X_{Au}}\right) + \frac{G_{Au}^{xs,(m)} - G_{Au}^{xs,B}}{\alpha_{Au}} \qquad (2)$$

where R is the gas constant, T is the temperature, σ_i is the surface energy, and α_i is the partial molar area of pure component i (i = Au or Ge). The terms $X_i^{(m)}$ and X_i are the mole fractions of a component i in the surface monolayer and bulk phase, respectively; $G_i^{xs,(m)}$ and $G_i^{xs,B}$ are the partial excess Gibbs energy of component i in the surface monolayer and bulk phase, respectively. Equation 2 can be solved using the bulk thermodynamic data for Au−Ge liquid binary reported by Okamoto,[12] the reported molar volume data for the pure components,[15] their reported surface energies,[16,17] and the coordination number ratio, $\beta = 0.83$, of atoms on the surface relative to those in the interior,[18] to obtain the equilibrium concentration of component i in the surface monolayer and the surface energy of the multi-

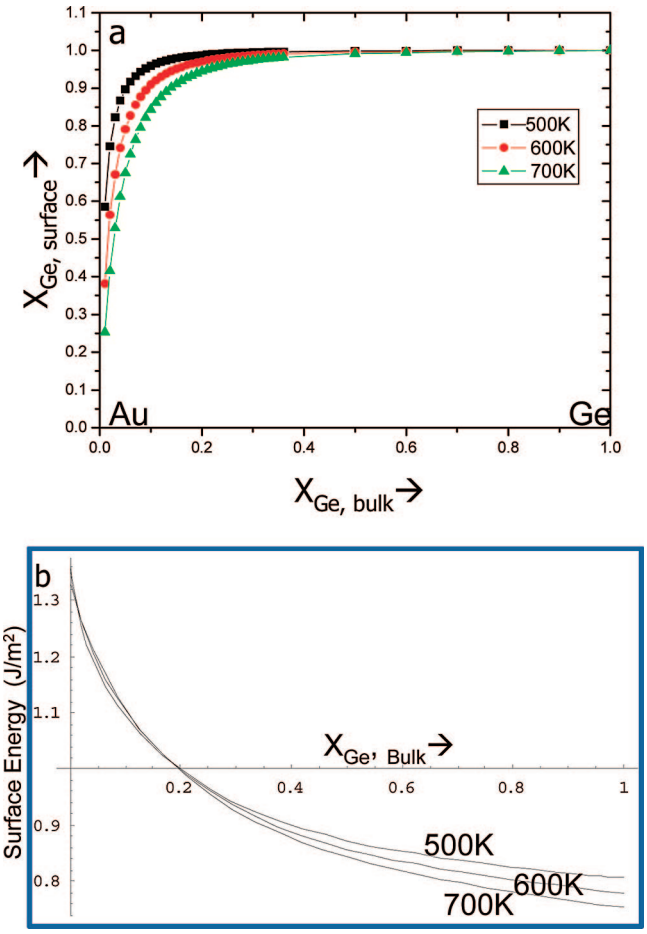

Figure 2. Surface monolayer composition and surface energy in Au−Ge liquid alloys. (a) Variation of surface monolayer composition *vs* the variation of the adjoining Au−Ge alloy phase. Because Ge has a much lower surface energy than Au, it segregates to the surface. (b) Variation of surface energy *vs* composition of the Au−Ge alloy phase. The surface energy of the liquid changes nonlinearly with bulk composition.

component alloy. These results for the liquid Au−Ge alloy phase are shown in Figure 2 for three different temperatures. It should be noted that the low surface energy of Ge relative to that of Au drives a very pronounced segregation of this component to the surface monolayer. This results in a departure from a linear "rule of mixtures" behavior of the composition-dependent surface energy in this binary system.

The Gibbs free energy of the various phases (diamond-cubic Ge, liquid or fcc Au solid solution) at the nanoscale case can be written as[13]

$$G^{(Ge)} = G^{B,(Ge)} + \frac{V^{(Ge)}\sigma^{(Ge)}}{r_L}$$

$$G^{(L)} = G^{B,(L)} + \frac{2V^{(L)}\sigma^{(L)}}{r_L}$$

$$G^{(Au)} = G^{B,(Au)} + \frac{2V^{(Au)}\sigma^{(Au)}}{r_{Au}} \qquad (3)$$

where $G^{(Y)}$ and $G^{B,(Y)}$ are the Gibbs free energy of phase Y in the nanoscale case and the bulk case, respectively, $\sigma^{(Y)}$ is the surface energy, $V^{(Y)}$ is the molar volume of phase Y, r_L is the radius of the liquid particle, and r_{Au} is the radius of gold solid solution. The radii of the liquid droplet (r_L) and the solid gold particle (r_{Au}) increase as they are saturated by Ge. The radius of the Ge NW is assumed to be same as the liquid catalyst droplet radius.

With the Gibbs free energies of the different phases (eq 3) calculated, one can evaluate the effective Au−Ge binary phase diagram at nanoscale dimensions. Such a phase diagram is shown in Figure 3. The eutectic temperature in the growth case for nanowires grown from 10, 20, and 40 nm diameter gold colloids is predicted to be 318, 338, and 349 °C, respectively (Table 1). These estimated eutectic temperatures are significantly larger than the observed Ge NW growth temperatures, which were as low as 270 °C under our experimental conditions. One notes that, under the assumptions made in the model, the liquidus curve for nanowires follows the bulk liquidus very closely in the Ge-rich side of the phase diagram. This can be understood because, with the number of Au atoms fixed by the size of solid Au nanoparticle, the diameter of the liquid alloy increases with the increase in Ge content, and the Gibbs–Thomson pressure terms in eq 3 become insignificant.

Nanowire nucleation when the catalyst particle is in contact with a flat Ge surface is different from nanowire growth when it is in contact with a Ge NW that has an effective radius of curvature Y_L. In the geometry of nanowire nucleation, a highly curved nanoparticle in contact with a flat substrate, the solid gold nanoparticle and the liquid alloy nanoparticle each experience (respectively) a Gibbs–Thomson pressure identical to that in the growth geometry, but the Ge substrate experiences no Gibbs–Thomson pressure. At the atomic level, Ge atoms at the periphery of the top terrace of a Ge nanowire are more active than those at kink sites on a nominally flat surface of solid Ge, so the temperature at which they equilibrate with the liquid is lower. The nucleation-geometry eutectic temperatures for nanowires grown from 10 and 40 nm diameter gold colloids are shown in Figure 3b along with the growth-geometry eutectics. We find that the nucleation-

TABLE 1. Predicted Eutectic Melting Points and Compositions in the Nanoparticle/Nanowire (NP/NW) Geometry for Surface Energy-Modified Au(fcc)/Liquid/Ge Phase Equilibrium *versus* the Nanowire Diameter

NP/NW diameter	10 nm	20 nm	40 nm
eutectic temperature	317.7 °C	338 °C	349 °C
Ge atom % of eutectic	0.271	0.275	0.277

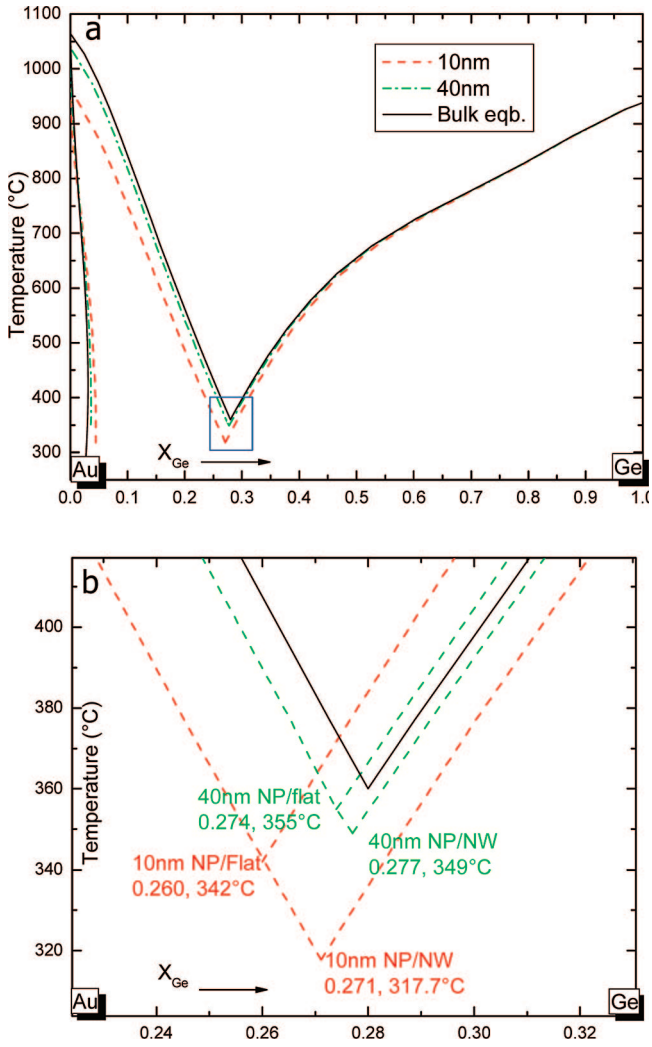

Figure 3. Equilibrium phase diagram for Au−Ge binary alloy system. (a) Comparison of eutectic formed during nanowire growth for nanowires synthesized from 10 and 40 nm diameter gold colloids to the bulk Au−Ge binary alloy eutectic. (b) Detail of the region represented by the squares in Figure 2a. Also shown with the growth geometry eutectics (liquid nanoparticle in contact with the nanowire, NP/NW) are the nucleation eutectics (liquid nanoparticle in contact with flat Ge, NP/flat) for 10 and 40 nm diameter nanowires.

geometry eutectic is close to the bulk eutectic temperature for both 10 and 40 nm nanowires, but the growth-geometry eutectic temperature is lowered by 42 and 11 °C, respectively. This result is consistent with our experimental observation that, in Au-catalyzed CVD synthesis of epitaxial Ge NWs, temperatures close to the bulk eutectic of Au−Ge (360 °C) are required for efficient nucleation of nanowires. However, it also means that capillary effects alone are unlikely to stabilize a Au−Ge liquid at the deep sub-eutectic temperatures often employed in Ge NW growth.[2,8]

Kodambaka *et al.*[8] recently proposed that Ge supersaturation of the Au−Ge liquid catalyst is responsible for the observation of VLS growth at temperatures far below the bulk eutectic. In their *in situ* TEM experiments, supersaturation was provided by Ge incorporated during decomposition of a digermane precursor which flowed through the electron microscope. Because germanium deposition occurred during imaging (the system may have been quite far from equilibrium), their results are not ideal for comparison with the equilibrium model developed above.

To test the predictions of the nanoscale phase equilibrium calculations, *in situ* heating and cooling studies of Ge NWs were performed inside a transmission electron microscope. A small cleaved piece of substrate was glued sideways to a TEM grid and mounted onto a heating stage. The temperature variations in the TEM annealing experiments parallel our two-temperature Ge NW deposition process used to synthesize epitaxial Ge NWs on Ge or Si single-crystal substrates. Therefore, they provide valuable details which may be related to the growth mechanism.

Temperatures close to the bulk eutectic were required for the Au catalyst particle on as-deposited 40 nm nanowires to melt *via* reaction with the Ge NW and form a eutectic liquid alloy during a heating cycle in the TEM. Melting was evidenced by (1) a loss of electron diffraction in both microdiffraction experiments and dark-field imaging of the particle (Figure 4a), (2) a loss of faceting (rounding) of the particle surface, and (3) a movement of the NW/catalyst interface toward the nanowire as Ge was incorporated and the catalyst particle volume increased. These observations are reasonably consistent with our prediction of a modest capillary lowering of the eutectic temperature (~10 °C for 40 nm diameter NWs) in this system. However, heat transfer by thermal conduction from the TEM hot-stage sample holder to the nanowire tips may produce an overestimation of the melting point in these experiments. Therefore, in addition to hot-stage TEM observations (Figure 4a), we have also studied the Au−Ge eutectic melting reaction by variable-temperature X-ray diffraction (XRD) in a high-purity inert (N_2 and argon) atmosphere (Figure 4b,c). Convective heat transfer through the gas ambient will supplement thermal conduction in the XRD experiments and thus may provide a more accurate measure of the eutectic melting point. Moreover, the XRD heating measurements sample a large number of catalyst particles simultaneously and thus yield better statistics than do hot-stage TEM studies. The heating rate was slow as the bulk eutectic melting point was approached. Heating across the range of temperatures depicted in Figure 4b,c while collecting XRD data took place over a period of several hours. Further experimental details for these catalyst melting experiments are described in the Supporting Information (section S2).

A marked decay of the Au (111) reflections is observed on heating 40 nm NWs to the temperature range 345−357 °C. The lowest temperature at which the decay is observed is consistent with the predicted surface-energy-modified eutectic melting point for this nominal wire diameter (see Figure 3 and Table 1). However,

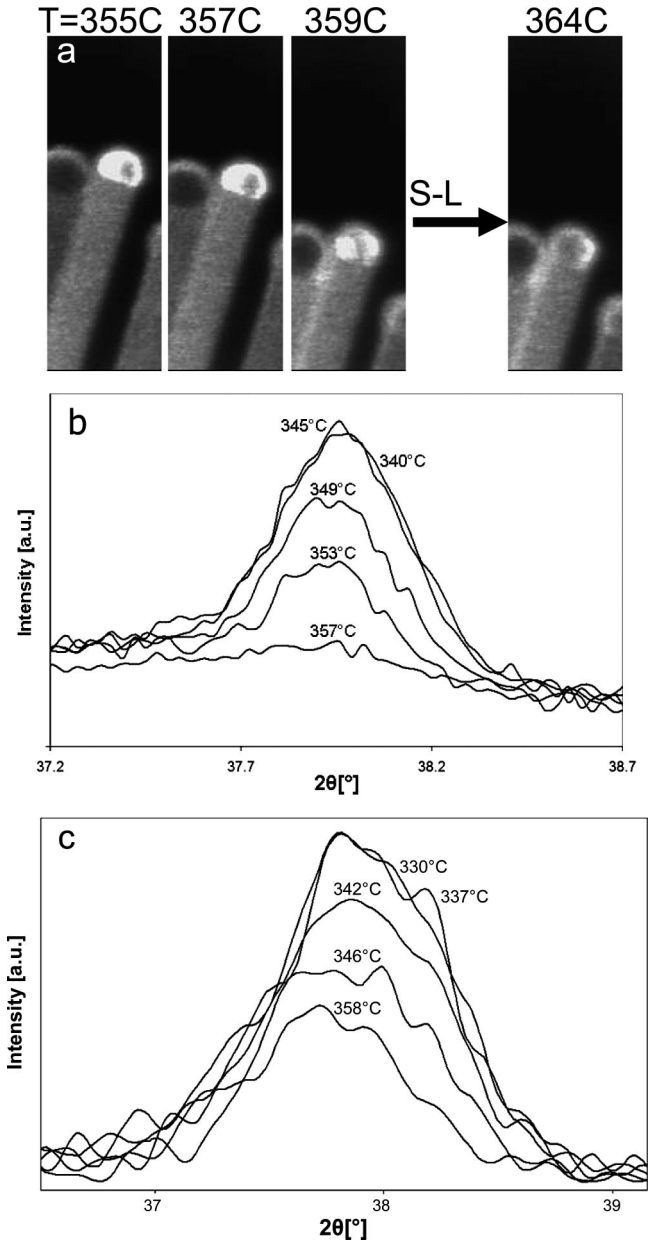

Figure 4. (a) Loss of diffraction contrast in the dark-field TEM image during heating of a Au catalyst particle on a 40 nm diameter Ge ⟨111⟩ NW to ~364 °C. (b) Diffracted intensity as a function of Ar annealing temperature for {111} Au reflection on 40 nm diameter Ge NWs. (c) Diffracted intensity as a function of Ar annealing temperature for {111} Au reflections detected from catalyst particles on 20 nm diameter Ge NWs.

coarsening of the Au nanoparticles, which appears to happen prior to wire nucleation on Ge and Si (111) surfaces, broadens the distribution of NW diameters relative to the initial Au colloid size distribution. Because the volume of the Au catalysts scales with the cube of their diameter, a substantial Au (111) diffracted intensity is expected for the relatively small fraction of Ge NWs that have diameters larger than the nominal value (in the case of Figure 4b, 40 nm). We believe that this is the reason that the decay in (111) Au peak intensity is not more abrupt during heating of the NP/NW samples in order to melt the catalysts.

In order to test the predictions of nanoscale phase equilibrium incorporating the relevant surface energies, we also studied Au catalyst melting on nominal 20 nm diameter Ge NWs. In this case, the attenuation of the (111) Au reflection on heating started at a temperature between 337 and 342 °C (Figure 4c), with further decay observed at higher temperatures. The behavior is qualitatively similar to that seen for NWs of 40 nm nominal diameter, but the peak width for the (111) reflection is larger for the 20 nm case (consistent with the broadening effect due to the smaller crystallite size), and the initial decay temperature is ~10 °C lower than that observed for the larger nanowires. The onset temperatures for Au (111) peak decay during heating are remarkably close to the theoretical values of the eutectic melting point in the NP/NW geometry (Table 1). The very close quantitative agreement must be considered fortuitous, given the assumptions made in the model and the uncertainty in the Au nanoparticle temperature on the XRD hot-stage. More significantly, the trend observed with decreasing NW diameter is consistent with the prediction of a modest decrease in eutectic melting point as a result of capillary effects. We also attempted hot-stage XRD measurements on NP/NW geometry samples with a nominal Au catalyst diameter of 10 nm; however, the (111) Au reflection obtained was too weak to accurately estimate the eutectic melting point, presumably due to the much smaller volume of each catalyst particle for this diameter and associated finite-size broadening of the Au reflections.

Crystallization of individual liquid Au−Ge catalysts was studied during cooling from above the melting point in the TEM. We found that the liquid alloy remained stable for undercoolings on the order of 100 °C. Crystallization of the Au−Ge liquid alloy was abrupt in an individual nanowire, as evidenced by a sudden retraction of the interface as Ge precipitated out of the liquid alloy onto the end of the Ge NW, which was frequently accompanied by the appearance of "ghost" diffraction contrast displaced from the tip image (Figure 5). The crystallization temperature of an individual nanowire varies in a very narrow range (±2 °C) during repeated heating/cooling cycles. We found that the liquid particles on the tips of different nanowires in a TEM specimen crystallize in the temperature range of 260−275 °C during slow cooling from temperatures above the melting point

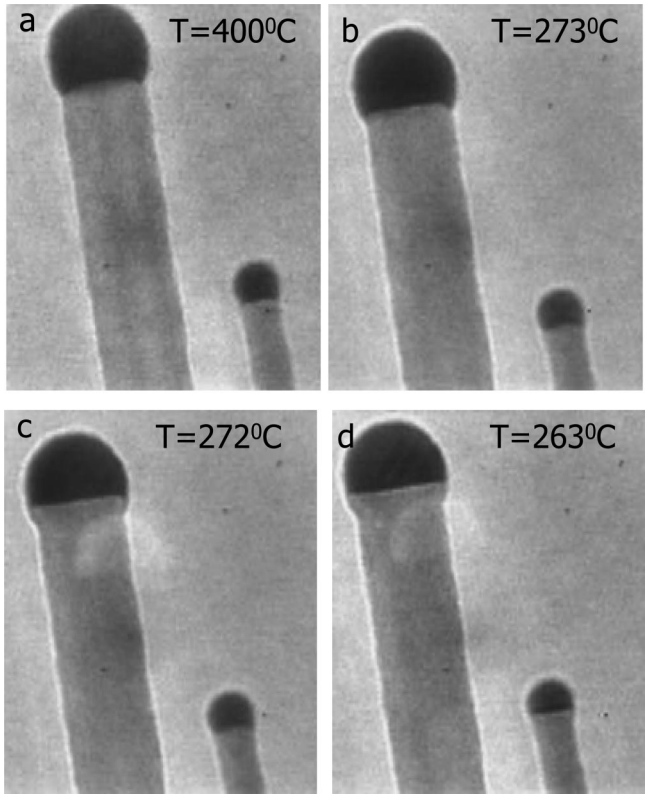

Figure 5. Cooling of nanowires inside the TEM after nanocatalyst melting. A substantial undercooling of the liquid below both the bulk and NW/NP eutectic temperature is observed. (a) Molten Au−Ge droplet at the tip of two nanowires. (b) Undercooled Au−Ge melt at the tip of nanowires just prior to crystallization. (c) Crystallization of Au−Ge tip in the larger-diameter nanowire. (d) Crystallization of Au−Ge tip in the smaller-diameter nanowire.

(see Supporting Information, section S2, for details). Interestingly, this temperature range is similar to the minimum temperature at which we have been able to grow Ge NWs by the two-temperature-step CVD process.

The variation of the crystallization temperatures of different nanowires within a specimen did not appear to be directly related to the diameter of nanowires in several specimens studied and may be an artifact of the differences in local heat transfer to and from the heating stage. Energy-dispersive X-ray spectroscopy performed in the TEM indicates that the solidified particles are nearly pure Au. The Au crystallites appear to lack any strong preferred crystallographic orientation with respect to the single-crystal Ge NWs both before and after a heating/cooling cycle. Prior to Au crystallization during cooling, the liquid/Ge NW interface was observed to retract in small increments, no more than a few Ge atomic layers in thickness at a time. This gradual, smaller-scale interface motion preceded the final, abrupt retraction of the interface associated with crystallization of the Au. The fact that this process of Ge transfer from the catalyst to the NW tip occurs prior to final Au solidification indicates that the supersaturation present during sub-eutectic cooling of the Au−Ge melt drives (and is at least partially consumed by) the nucleation of Ge (111) steps on the NW growth facet. These results, therefore, appear to confirm the hypothesis advanced by Kodambaka *et al.*[8] that a substantial Ge supersaturation, which tends to stabilize the melt at low temperatures, is necessary to drive Ge transfer from the liquid catalyst to the Ge NW tip. However, the abrupt and larger-scale, final interface motion simultaneously requires additional Ge transfer to the NW *and* the nucleation of solid Au from the liquid.

The solidification and melting behavior of the Au−Ge nanocatalysts differ from that reported recently by Kodambaka *et al.*[8] in that those authors reported a modest size dependence of catalyst crystallization at a given temperature and digermane precursor flow, which is at odds with the predictions of a capillary lowering of the effective nanowire/nanoparticle eutectic. In their experiments, smaller-diameter catalysts were found to crystallize more rapidly at a given sub-eutectic growth condition than larger catalysts. This observation may be a consequence of the Ge supersaturation of the Au−Ge liquid catalyst under nanowire growth conditions. Perhaps more significantly, we also did not observe the large (~50 K) superheating above the bulk eutectic, which Kodambaka *et al.*[8] reported was necessary to re-melt Au−Ge catalysts after their solidification in the TEM. Both our hot-stage TEM and XRD experiments indicate that melting occurs close to the calculated capillary-modified eutectic temperatures and somewhat below the bulk eutectic for Au−Ge. Indeed, given the very large and positive heat of mixing exhibited by Ge and Au in the solid phases (implying a substantial solid Au/solid Ge interface energy) and the larger average surface energy of the solids compared to that of the liquid phase, a substantial superheating for eutectic melting in this system would be unexpected.

Our TEM cooling results are consistent with both a kinetic barrier to Ge (111) step nucleation on the growth facet (as evidenced by gradual interface retraction prior to solidification and as proposed by Kodambaka *et al.*[8]) and a kinetic barrier for final nucleation of solid Au from the liquid. We have used classical nucleation theory to further examine the latter possibility. For container-less solidification of Au in the liquid catalyst droplet at the tip of a Ge NW, heterogeneous nucleation of Au is unlikely. In fact, nanoscale catalyst particles at the tips of nanowires mimic small liquid droplets which are often studied in research on homogeneous nucleation.[19] Furthermore, as noted above, Ge segregates strongly to the surface of the liquid, thus rendering the liquid/vapor interface unsuitable as a nucleation site for Au. Finally, the necessity of maintaining a local Ge supersaturation in the liquid near the interface with Ge to drive nucleation of steps on the Ge NW (111) growth facet may inhibit heterogeneous nucleation of solid Au on the Ge NW (111) facet.

We have calculated the homogeneous nucleation rate of solid Au in a Au−Ge liquid alloy using classical nucleation theory. The nucleation rate was calculated from the number of critically sized nuclei present at a particular undercooling, as described in the Supporting Information (section S3). Figure 6 depicts the range of homogeneous nucleation rates predicted as a function of temperature, for reasonable values of the important kinetic parameters in the nucleation rate equation. The most uncertain parameters needed to predict the nucleation rate are the effective supersaturation of Ge in the liquid, compared to the metastable liquidus composition at a given experimental undercooling, and the effective activation enthalpy for Au atom migration from the liquid to the embryonic Au nucleus. Figure 6 depicts the probable range of nucleation rates that would be expected in this system between two limiting conditions of (1) no supersaturation (X_{Ge} is the liquidus composition at a given undercooling) and a small atom migration enthalpy of 0.5 eV, and (2) maximum supersaturation (X_{Ge} = 0.277, the NP/NW geometry eutectic composition) and a large atom migration enthalpy of 1.5 eV. A single data point representing the approximate rate and range of temperatures for Au nucleation estimated from our experiments is also shown on the figure, and it falls within the bounding curves associated with these two limiting cases. Figure 6 indicates the extent to which Ge supersaturation of the liquid, resulting from slow kinetics of transfer of Ge atoms from the liquid to the (111) NW face, can suppress the homogeneous nucleation rate of the Au. In keeping with our experimental data, the results in Figure 6 indicate that this can occur even without intentional addition of Ge to the system as in NW growth. Moreover, even without Ge supersaturation (the upper curve in Figure 6), the barrier to forming a Au nucleus within the liquid is such that homogeneous nucleation of the Au catalyst within the ~40 nm diameter Au−Ge liquid nanoparticle is unlikely to occur at temperatures much above 310–320 °C on experimentally accessible

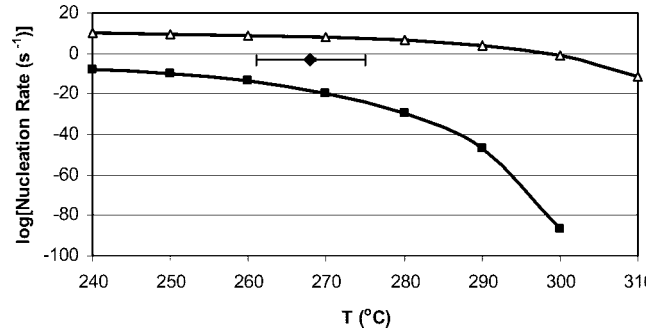

Figure 6. Log_{10}[nucleation rate] for gold crystallization in a 40 nm diameter hemispherical Au−Ge binary liquid alloy as a function of temperature. The top curve (△) shows predicted the nucleation rate for an effective activation enthalpy of atom migration of 0.5 eV if the liquid composition follows the metastable extension of the high-temperature L−Ge liquidus (see Figure 3). The lower curve (■) shows the rate for an atom migration enthalpy of 1.5 eV, assuming a fixed liquid composition of 27.7 atom % Ge, consistent with the NP/NW eutectic for this wire diameter. A data point (◆) representing results observed in multiple cooling experiments performed in the TEM on 40 nm diameter Ge NWs is also shown.

time scales. Our results indicate, therefore, that both Ge supersaturation of the liquid droplet and the Au nucleation barrier likely contribute to the observed hysteresis of the melting and solidification temperatures.

To summarize, we have shown that thermodynamic arguments based on depression of the binary eutectic temperature through capillary effects should not stabilize Au−Ge liquid catalysts of >10 nm diameter at the deep sub-eutectic temperatures often employed in the growth of Ge NWs using Au catalysts. Germanium supersaturation of the Au−Ge droplet, required to drive the transfer of Ge atoms from the liquid to the NW tip, and the energetic barrier associated with homogeneous nucleation of solid Au appear, however, to be sufficient for the existence of liquid catalyst nanoparticles at very large undercoolings relative to the bulk eutectic. Formation of similar metastable, low-temperature liquids may effectively catalyze sub-eutectic VLS growth in other nanowire systems, beyond Au−Ge.

METHODS

The Ge NWs used in this study were grown using colloidal gold particles (Sigma Aldrich Chemical Co., nominal particle diameter = 10, 20, and 40 nm) as the catalysts. Nanowire growth was carried out in a cold-wall, lamp-heated, CVD chamber by a two-temperature process, details of which are given elsewhere.[2] The procedures for XRD and TEM hot-stage experiments are described in detail in the Supporting Information.

Supporting Information Available: Estimation of the surface energy of multi-component solution in nanostructured systems, special procedures for XRD and TEM hot-stage experiments, and calculation of homogeneous nucleation of solid Au in Au−Ge liquid. This material is available free of charge *via* the Internet at http://pubs.acs.org.

REFERENCES AND NOTES

1 Wang, D. W.; Wang, Q.; Javey, A.; Tu, R.; Dai, H. J.; Kim, H.; McIntyre, P. C.; Krishnamohan, T.; Saraswat, K. C. Germanium Nanowire Field-Effect Transistors With SiO2 And High-K HfO2 Gate Dielectrics. *Appl. Phys. Lett.* **2003**, *83*, 2432–2434.

2 Adhikari, H.; Marshall, A. F.; Chidsey, C. E. D.; McIntyre, P. C. Germanium Nanowire Epitaxy: Shape and Orientation Control. *Nano Lett.* **2006**, *6*, 318–323.

3 Wang, D. W.; Dai, H. J. Low-Temperature Synthesis of Single-Crystal Germanium Nanowires by Chemical Vapor Deposition. *Angew. Chem., Int. Ed.* **2002**, *41*, 4783–4786.

4 Jagannathan, H.; Deal, M.; Nishi, Y.; Woodruff, J.; Chidsey, C.; McIntyre, P. C. Nature of Germanium Nanowire Heteroepitaxy on Silicon Substrates. *J. Appl. Phys.* **2006**, *100*, 024318.

5 Wagner, R. S.; Ellis, W. C. Vapor Liquid Solid Mechanism of Single Crystal Growth. *Appl. Phys. Lett.* **1964**, *5*, 89–90.

6 Kamins, T. I.; Li, X.; Stanley Williams, R.; Liu, X. Growth and Structure of Chemically Vapor Deposited Ge Nanowires on Si Substrates. *Nano Lett.* **2004**, *4*, 503–506.
7 Wu, Y.; Yang, P. Direct Observation of Vapor-Liquid-Solid Nanowire Growth. *J. Am. Chem. Soc.* **2001**, *123*, 3165–3166.
8 Kodambaka, S.; Tersoff, J.; Reuter, M. C.; Ross, F. M. Germanium Nanowire Growth Below the Eutectic Temperature. *Science* **2007**, *316*, 729–732.
9 Greytak, A. B.; Lauhon, L. J.; Gudiksen, M. S.; Lieber, C. M. Growth and Transport Properties of Complementary Germanium Nanowire Field-Effect Transistors. *Appl. Phys. Lett.* **2004**, *84*, 4176–4178.
10 Tutuc, E.; Guha, S.; Chu, J. O. Morphology of Germanium Nanowires Grown in Presence of B2H6. *Appl. Phys. Lett.* **2006**, *88*, 043113.
11 Borel, J.-P. Thermodynamical Size Effect and the Structure of Metallic Clusters. *Surf. Sci.* **1981**, *106*, 1–9.
12 Okamoto, H.; Massalski, T. B. *Bull. Alloy Phase Diagrams* **1984**, *5*, 600–610.
13 Lupis, C. H. P. *Chemical Thermodynamics of Materials*; North Holland: New York, 1983; Vol. 35, pp 352–353
14 Butler, J. A. V. The Thermodynamics of the Surfaces of Solutions. *Proc. R. Soc. A* **1932**, *135*, 348–375.
15 Iida, T.; Gutherie, R. I. L. *Physical Properties of Liquid Metals*; Oxford Science Publishers: New York, 1988; pp 70–72.
16 Iida, T.; Gutherie, R. I. L. *Physical Properties of Liquid Metals*; Oxford Science Publishers: New York, 1988; pp 133–134.
17 Lupis,C. H. P. *Chemical Thermodynamics of Materials*; North Holland: New York,1983; p 380.
18 Tanaka, T.; Hack, K.; Iida, T.; Hara, S. Application of Thermodynamic Databases to the Evaluation of Surface Tensions of Molten Alloys, Salt Mixtures and Oxide Mixtures. *Z. Metall.* **1996**, *87*, 380–389.
19 Perepezko, J. H.; Paik, J. S. Thermodynamic Properties of Undercooled Liquid Metals. *J. Non-Cryst. Solids* **1984**, *61−62*, 113–118.